Advanced Raman Spectroscopies for Exploring Bio-systems

Giulia Rusciano[1] and Antonio Sasso[1*]

Presentata dal socio Leonardo Merola
(Adunanza del 18 dicembre, 2015)

Keywords: Raman spectroscopy, Surface- and Tip-Enhanced Raman Scattering, Biophotonics

ABSTRACT - Raman spectroscopy has experienced a renewed development for the huge potentiality offered by the plasmonics, a new area of nano-physics concerning the enhanced response of metal nanostructures to optical fields. Here we review the basic principles of these novel Raman spectroscopies focusing on a selection of experiments performed in our laboratories during the last recent years.

RIASSUNTO - La spettroscopia Raman ha ricevuto un rinnovato sviluppo per le potenzialità offerte dalle plasmonica, una nuova area della nano-fisica che riguarda la risposta di nanostrutture metalliche irradiate a campi ottici. In questa nota intendiamo riportare una breve rassegna sui principi di base di queste nuove tecniche Raman concentrandosi su una selezione di esperimenti condotti nel corso degli ultimi anni nei nostri laboratori.

[1]Universita' di Napoli *"Federico II"*, Dipartimento di Fisica "*Ettore Pancini*", Via Cintia, **8**0126 Napoli.
[*]To whom correspondence should be addressed: sasso@na.infn.it

1- INTRODUCTION

Biophotonics is an emerging area of scientific research, involving the use of light to detect and manipulate biological materials [Pavesi and Fauchet, 2008]. Its mission is to understand the inner workings of single microorganisms, or even single bio-macromolecules, in a non-invasive way. This approach has recently allowed to shed light on the peculiar function of single proteins, DNA and other important molecules. In medicine, the advent of biophotonics has introduced new ways to image and analyze living microorganisms, in order to detect, diagnose and treat diseases.

For biological samples, confocal, laser-based fluorescence microscopy has been traditionally considered as the golden standard for optical imaging due to its high sensitivity and facile preparation of samples (staining). Generally, fluorescence imaging is achieved by using fluorophores that selectively bind to target molecules. However, all fluorescence-based techniques present several shortcomings, such as photobleaching and photoblinking of the fluorescent labels, interference of fluorophores with the marked molecules and, most importantly, the quite poor chemical selectivity of fluorescence spectra.

Raman Spectroscopy (RS) has recently emerged as a formidable alternative to fluorescence, potentially capable to overcome fluorescence's drawbacks, as demonstrated by the increasing number of applications in many fields of life sciences. Raman Spectroscopy assesses the chemical composition of a sample by exploiting the inherent and unique vibrational structure of molecular bonds in the sample (chemical fingerprinting).

In this brief review we present some applications of RS to biological systems. We start from the conventional RS, discussing the basic principle and the main limits. Afterwards, we discuss recent variants of this spectroscopic technique based on the excitation of plasmon resonances in metal nanostructures (Surface Enhanced Raman Scattering, SERS). Finally, we present the frontiers of modern Raman-based techniques, which allows to acquire a spatial resolution that is outside of the diffraction-limited regime of the conventional optical techniques. plasmonics-based Raman discussing of a novel technique which combine the nanometric resolution of the Atomic Force Microscopy with the plasmonics resonance localized at the tip itself of the AFM.

2. BASIC PRINCIPLES OF RAMAN SPECTROSCOPY

In the photon picture, scattering of light can be seen as an elastic or inelastic collision between an incident photon and a molecule (see Fig.1): the molecule undergoes an excitation to a virtual state followed by a nearly

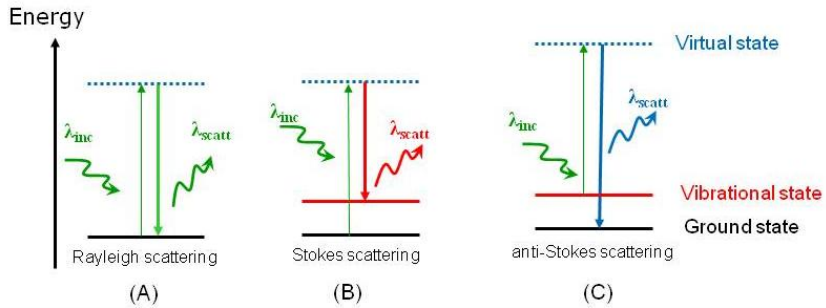

Figure 1: Energy level diagram for Rayleigh, Stokes, and anti-Stokes Raman scattering.

simultaneous de-excitation towards the initial energy level (elastic) or a vibrational level different from the initial one (inelastic). The scattering event duration is of the order of an optical cycle, i.e. it occurs in 10^{-14} s or less. Moreover, since virtual states are created only when photons interact with electrons, the energy of these states is determined by the frequency itself of the incident photons. From the virtual state, molecules may decay following three different paths. Most of them return back to the initial state through the emission of a photon having the same energy of the incident photon (see Fig.1A). This process, named Rayleigh scattering, is, for instance, the reason for the blue colour of the sky caused by the scattering of sunlight in the atmosphere. Another possibility is that the molecule decays toward an excited vibrational level (see Fig.1B): in this case the energy photon is lower than the incident one and the energy defect is released to the internal (vibrational) energy of the molecule. This process is called Stokes scattering. Hence the energy difference between the initial and final vibrational levels (Raman shift) expressed in wavenumbers $\tilde{\nu}$ (cm^{-1}), is given through the relation:

$$\tilde{\nu} = \frac{1}{\lambda_{inc}} - \frac{1}{\lambda_{scat}} \qquad (1)$$

in which λ_{inc} and λ_{scat} are the wavelengths of the incident and Raman scattered photons, respectively. Finally, a third process can take place when we consider molecules in an excited vibrational level. In this case a molecule excited in a virtual state can decay in the ground state (see Fig.1C). This process, called anti-Stokes scattering, produces photons with energy higher that the incident ones: the energy defect is now transferred from the molecules to the photons. Nevertheless, since the number of molecules in an excited vibrational level decreases as $e^{-\frac{\Delta E}{kT}}$ (Boltzmann statistic), anti-Stokes scattering is much less probable than the Stokes scattering (typically by a factor around 1000). For this

reason, Raman analysis is usually limited to the observation of the Stokes scattering.

From an experimental point of view, a Raman spectrum is obtained by dispersing the scattered photons by means of diffraction gratings, rejecting the intense elastic scattered light by a notch filter, and recording the several peaks by means of a sensitive CCD camera. Since different molecules have bonds vibrating at well-defined frequencies, it turns out that the Raman spectrum consists of quite sharp peaks representing the actual "*chemical fingerprint*" of the molecule.

When RS is combined with confocal optical microscopy (*micro-RS*) a spatial resolution of ~300 nm in the transverse x-y plane and of ~1.2 μm in the axial direction can be achieved. Clearly, for extended samples, it is possible to acquire the Raman spectra on a two- or three-dimensional array of points, with a step comparable with the spatial resolution (*Raman imaging*). Therefore, the information carried by the acquired spectra can be represented by 2D images (or 3D profiles), reporting the spatial variation of a given Raman parameter. This parameter is usually the intensity of a particular Raman band, but sometimes it derives it from a more complicated analysis of the whole Raman spectrum.

Nowadays *Raman imaging* is becoming a tool for a patchwork of interdisciplinary researches, involving physicists, chemists and biologists, as well as molecular biologists and clinicians.

The Raman spectrum provides essentially the same type of information as the infrared (IR) absorption spectrum, i.e. the vibrational energies of molecular normal modes of vibration. However, the two techniques have experienced a quite different fortune for biological applications. This is mainly due to the strong IR-absorption cross section of water, which usually mask the contribution of species in aqueous environment. In contrast, water interferes only poorly with Raman spectra of aqueous solutions, due to the quite low water Raman activity. The other side of the coin of RS is its very low efficiency caused by the small cross-section of the inelastic scattering process, up to 12 orders of magnitude smaller than fluorescence. This makes Raman detection of molecules at sub micro-molar concentration prohibitive.

3. RESONANT RAMAN SPECTROSCOPY OF SINGLE RED BLOOD CELL MANIPULATED BY OPTICAL TWEEZERS

When the frequency of the Raman probe is close to the frequency of an electronic transition, the Raman scattering cross section is enhanced by 3-6 order of magnitude. This effect, which greatly improves the sensitivity of RS, is referred to Resonance Raman Scattering (RRS). RRS has been observed for several classes of biologically important molecules, such as metalloporphyrins

and carotenoids, which exhibit strongly allowed electronic transitions in the visible region due to the presence of a chromophor. The enhanced contribution from selected chromophoric moieties can be used to selectively pick out and positively identify a molecule in a matrix. This is the lucky case of haemoglobin (Hb), the main component of Red Blood Cells (RBC).

As a matter of facts, the chromophoric structure of the heme, the functional group of Hb which links oxygen in lungs and realises it throughout the body, results in a strong enhancement of the Raman Scattering using laser wavelengths close to the heme electronic absorption bands. This allows the investigation of Hb within erythrocytes without interference by the scattering from other cellular component.

The Hb structure is characterized by two states: an oxygenated, relaxed structure (R or oxy state) and a de-oxygenated or tense structure (T or de-oxy state). Intriguingly, these two state are well distinguishable by RRS, due to the presence of specific Raman bands which are quite sensitive to spin state of iron according if this atom is bond to oxygen or to carbon dioxide, as shown in Fig. 2 [Rusciano, 2010]. This feature has expired numerous studies, aimed at shedding light on the response of Hb to external stimuli and/or to reveal Hb-related disorders, even at level of single cell.

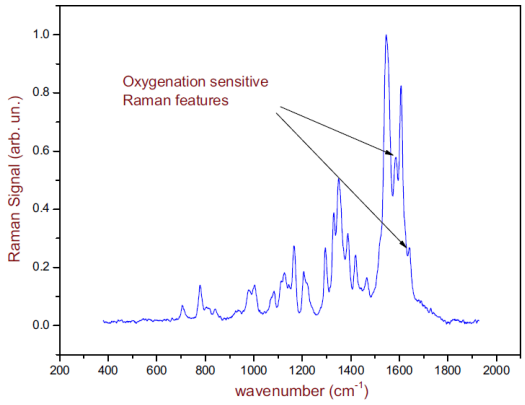

Figure 2: **Raman spectra of Hemoglobin.**
The peaks in the range 1500-1700 cm^{-1} are sensitive to the oxy- or deoxy state. In particular, the two peaks highlighted by the arrows represent two significant vibrational modes of Hb used in our analysis.

Recently, we have demonstrated that RRS is able to investigate the process of oxygen release from Hb occurring in the body circulatory system [De Luca et al., 2008]. Historically, the deformation of RBCs when they pass through small microcapillaries has been thought as the main channel where Hb oxy-deoxy

transition occurs. In particular, numerical simulations show that Hb deoxigenation under RBC stretching is due to the necessity to pack Hb in a smaller volume and the contemporary enhanced hemoglobin-membrane interactions. However, the strict connection between RBCs deformation and Hb de-oxygenation was never proven before. RRS, combined with the use of an Optical Tweezers (OT), gave us the opportunity to reach this goal. OTs are based on the use of strongly focused laser beams, allowing manipulation of single cells in absence of any mechanical contact. A sketch of our experimental approach is shown in Fig. 3A where a single RBC is immobilized at two its ends by two OTs, used as handles to manipulate the cell.

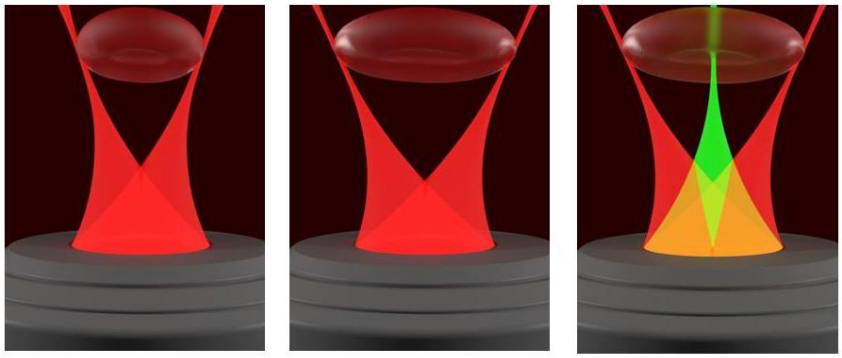

Figure 3: Manipulation and stretching of a single RBC

A single red blood cell is handle by two optical traps at its two ends using a near infrared laser, λ=1064 nm (part A). By translating the traps the cell is stretched (part B). A third laser, emitting at 532 nm, is used as Raman probe (part C).

Afterwards, the RBC is stretched by increasing the distance between the traps (Fig.3B). Finally, RBC was relaxed by reporting the cell to its natural, un-stretched state. Besides the two laser traps (emitting in the near infrared, λ=1064 nm), a third laser (emitting in the visible, λ=532 nm) is employed as Raman probe (Fig.3C). At each step of the cell elongation, Hb oxygenation state is monitored by recording the Raman spectrum collected from the same region of the trapped cell. From the analysis of the resulting spectra, it turns out that, under stretching, Hb undergoes transition to the deoxygenated state. After stretching, RBC recovers its initial shape together with its initial oxygenation state. Although optical stretching of a floating RBC is only a poor simulation of folded-elongated RBCs within capillaries, our study constitutes the first experimental evidence of the de-oxygenation of Hb inside RBCs under the

application of a mechanical deformation. This result is quite interesting from a physiological point of view, contributing to understand how oxygen transfer occurs in human body.

Deficiency in Hb oxygenation capability are common to many blood disorder, including thalassemia. Thalassemia is a disease of RBC inherited as a semidominant trait, quite diffuse in the populations of the Mediterranean sea. In thalassemia, the genetic defect results in reduced rate of synthesis of one of the globin chains composing the heme group.

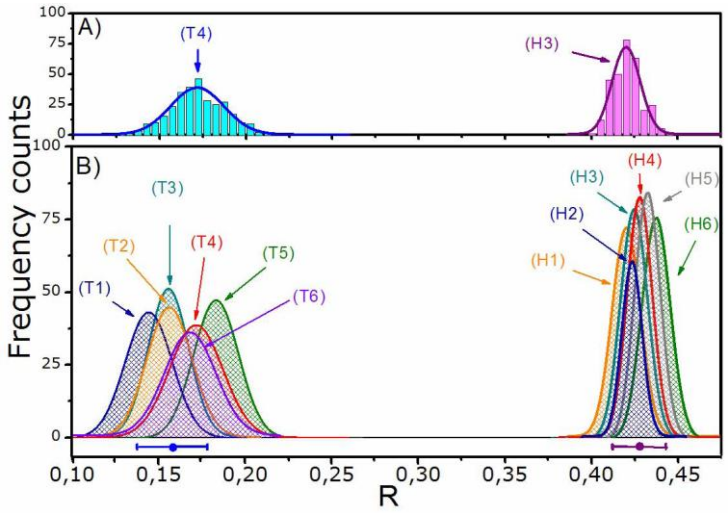

Figure 4: Analysis of healthy and thalassemic RBCs.
Statistical distributions of the ratio $R=I_{37}/I_{11}$ obtained by analyzing 300 RBCs from a single normal (pink histogram) and thalassemic (blue histogram) donor. The fitting of these distributions with Gaussian profile is also shown. B: Gaussian profiles obtained by fitting the experimental distributions relative to 6 normal (Hi) and 6 thalassemic (Ti) volunteers. The weighted-mean and the standard deviation for the two kinds of cells are evidenced by horizontal bars.

So far, we have investigated the effects of thalassemia, at single cell level, using a Raman system. By resonant excitation of hemoglobin Raman bands, we have examined the oxygenation capability of β-thalassemic erythrocytes. Fig. 4, part a, shows the statistical distributions (over 300 measurements) of the ratio $R=I_{37}/I_{11}$ between two selected Hb Raman bands, the first being sensitive to Hb oxygenation.
As it is possible to note, this ratio completely differentiates RBCs from obtained by analyzing 300 RBCs from a single normal (pink histogram) and thalassemic (blue histogram) donor. Part b of Fig. 4, instead, shows the Gaussian profiles obtained by fitting the experimental distributions relative to 6 normal (Hi) and 6

thalassemic (Ti) volunteers. These results demonstrate that our approach may have potential for the monitoring of blood diseases.

4. BASIC PRINCIPLE OF SURFACE ENHANCED RAMAN SCATTERING

A huge step forward to the concrete use of Raman spectroscopy in biosciences is due to the discovery of the huge enhancement (up to 12 orders of magnitudes) of the Raman signal when the analyte under investigation is close to proper nano-sized metallic particles (NPs). This phenomenon is called Surface-Enhanced Raman Scattering (SERS) and, since its discovery, its use as analytical technique has grown exponentially [Rusciano et al., 2011].
Historically, SERS birth dates backs to 1974 when Fleishmann and co-workers [Fleischmann et al, 1974] observed an anomalous enhancement of the Raman signal for pyridine molecules adsorbed over a roughened silver surfaces. Few years later two independent papers [Jeanmaire and Van Duyne, 1977, Albrecht and Creighton, 1977] provided the first physical interpretation based on Localized Plasmon Resonance (LPR) induced by the laser radiation shining the nanostructured metal surface.

As the simplest model to describe LPR we can assume a small metal sphere illuminated by the light. The time-varying electromagnetic (EM) field of the illuminating light can sustain collective oscillating surface plasmonic multipoles. If the size of the metallic structure is small compared to wavelength of incident light, the plasmonic wavepacket will remain confined in the nanostructure and it will give rise to a surface plasmon (SP). Moreover, if the frequency of incident EM field is close to the SP oscillation frequency, the field extinction, i.e. absorption and scattering, will reach a maximum. It is not difficult to image that the SP resonance depends critically not only by the NPs size and shape but also by the dielectric function of the bulk metal and by the surrounding material. This is the reason for which, although the gold bulk plasma frequency is in the UV region, the SP frequency for a gold NP lies in the green region (near 520 nm). This scattering property have attracted considerable interest since historical times when metallic NPs were used as decorative pigments in stained glasses and artworks. The most famous example of such application is the famous Lycurgus Cup is a 4^{th}-century Roman glass cage cup, which exhibits a different colour depending on whether or not light is passing through it. To get an idea into the origin of SP resonances in metallic nanostructures, we have no other options but to actually solve Maxwell's equations with appropriate boundary conditions. A useful approximation scheme for this purpose is the so called electrostatic approximation, in which the electric field of the light is considered to be constant over distances comparable to the object size so that any phase delay of the field is neglected. In

practice, for visible radiation, the electrostatic approximation works well for objects of typical sizes up to ~10 nm. Fully analytical solutions of Maxwell equations exist in a few selected simple geometries (Mie theory). The sphere is one of these cases. In such case, it is possible to demonstrate that the electrostatic boundary conditions on the sphere can be satisfied by considering the total EM field as the superposition of that produced by an induced dipole at the origin (p) with the external applied field (E). The induced dipole is given by:

$$\alpha = \varepsilon_m V \frac{\varepsilon - \varepsilon_m}{\epsilon + 2\varepsilon_m} \qquad (2)$$

where V is the particle volume, $\varepsilon = \varepsilon_r + i\varepsilon_{im}$ is the complex frequency-dependent dielectric function of the metal, and ε_m is the dielectric constant of the surrounding medium. Starting from Eq. (1), SERS enhancement mechanism can be simply described with the diagram of Fig. 5.

As a matter of facts, a molecule in proximity of the sphere (at distance *d*) is exposed to a field E_{tot}, which is the superposition of the incoming field E_0 and the field of the dipole, E_{dip}, induced in the metal nanosphere. This field assumes the form:

$$E_{tot} = E_0 + E_{dip} = E_0 + r^3 \frac{\varepsilon - \varepsilon_m}{\varepsilon + 2\varepsilon_m} E_0 \frac{1}{(r+d)^3} \qquad (3)$$

It is possible to define an enhancement factor (EF) as ratio of the total field E_{tot} at the molecule position and the incoming field E_0:

$$A(\nu_L) = \frac{E_{tot}}{E_0} \sim \frac{\varepsilon - \varepsilon_m}{\varepsilon + 2\varepsilon_m} E_0 \left(\frac{r}{r+d}\right)^3 \qquad (4)$$

The most important feature of the previous equation is the presence of the denominator $\varepsilon + 2\varepsilon_m$. In fact, assuming $\varepsilon_{im} \sim 0$ (low metal absorption), a strong resonance occurs when at the laser frequency ν_L the condition $\varepsilon_r = -2\varepsilon_m$ is satisfied. In an analogous fashion, the Stokes and anti-Stokes fields

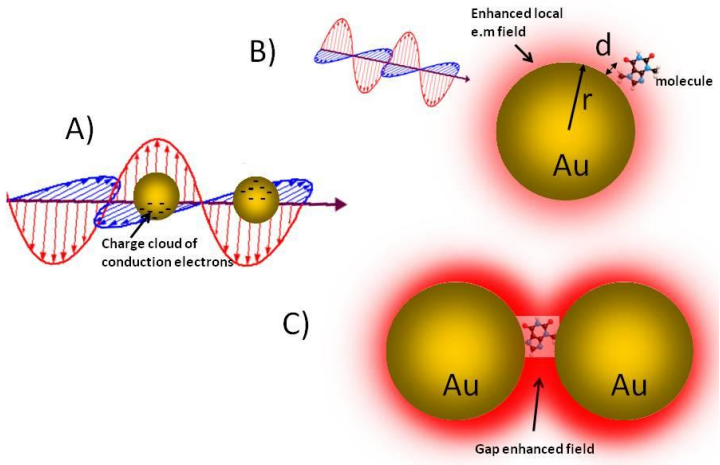

Figure 5: Cartoon of SERS mechanism.
Simple description of SERS: a) a metal nanoparticle illuminated by light gives place to oscillation of the free electrons of the surface; b) a molecule placed at nanometric distance d from the NP surface is affected by an amplified optical field; c) amplification if further increased (hot-spot) in the gap region in dimer structure.

will be enhanced too, if they are in resonance with surface plasmons of the sphere. Therefore, taking into account both effects, the electromagnetic enhancement factor for the Stokes signal is:

$$G = |A|^2|A|^2 \sim E_0^4 \left|\frac{\varepsilon(\nu_L) - \varepsilon_m}{\varepsilon(\nu_L) + 2\varepsilon_m}\right|^2 \left|\frac{\varepsilon(\nu_S) - \varepsilon_m}{\varepsilon(\nu_S) + 2\varepsilon_m}\right|^2 \left(\frac{r}{r+d}\right)^{12} \qquad (5)$$

being ν_S the frequency of the inelastically scattered photon. This formula shows that the EM enhancement factor scales as the forth power of the local field and reaches its maximum when both excitation and Stokes field are in resonance with the plasmons. Moreover, electromagnetic enhancement is effective when the analyte is very close to the nanostructure, as G decreases as $(1/d)^{12}$, which is responsible of the local character of SERS enhancement.

For noble metals (gold, silver, and copper) the resonance condition can be satisfied at visible frequencies, where they exhibit a negative dielectric function and low absorption. It is worth noticing that, in the electrostatic approximation, the plasmon frequency of a nanosphere does not depend by its actual size. Nevertheless, the conditions under which the electrostatic approximation represent the real solution of the problem (the solution of Maxwell's equations)

is limited by applicability range of the electrostatic approximation. For larger NPs, the size effect on the resonances can be observed. As general rule, as the size increases, the NPs resonances (i) shift to the red, (ii) are strongly damped and spectrally broadened, and (iii) new resonances appear, which are typically related to the activation of multipolar resonances (such as quadrupolar resonance). An additional level of complexity, but also of great interest, of the plasmonic resonances arises from the existence of coupled plasmon resonances for two or more closely spaced objects. Considering, for instance, the very simple case of two metallic nanobeads, it is possible to demonstrate that resonance coupling produces a red shift of the plasmon resonance, with its intensity mainly concentrated in the middle of the two beads. This gap effect is illustrated in Fig.5c.

The enhancement effect just described is commonly referred as "electromagnetic enhancement". However, SERS effect has also a strong molecular selectivity and a clear dependence on the chemical nature of the Raman molecule. This suggests the existence of an additional chemical SERS enhancement mechanism. Among the different mechanisms proposed to explain this chemical effect, the charge transfer mechanism is the most reliable. In particular, it is described as a four steps process, involving the transfer of a charge from the metallic nanostructure and back. In general, the chemical SERS enhancement mechanisms contribute to the enhancement by a factor of $10 - 10^3$.

5. SERS SUBSTRATES OF HIGH SPATIAL REPRODUCIBILITY FOR IMAGING OF CELL MEMBRANES

Label-free chemical imaging of live cell membranes can shed light on the molecular basis of cell membrane functionalities and their alterations under membrane-related diseases. In principle, this can be done by surface-enhanced Raman scattering (SERS) in confocal microscopy, but requires engineering plasmonic architectures with a spatially invariant SERS enhancement factor G. This requirement has opened new research area in nanoplasmonic, aimed at producing nano-structured surface showing high efficiency and reproducibility. SERS substrates can be grouped in three main categories: i) metal NPs in suspension; ii) metal NPs immobilized on solid substrates; iii) nanostructures fabricated directly on solid substrates, which includes nanolithography and template synthesis of nanostructures. The variety of SERS substrates reported in recent years is enormous and obviously it is not possible to review the whole field herein. Rather, we prefer to discuss a method developed in our laboratory that seems to combine the main expectations for realistic application of SERS to bio-system. We took advantage of the use of the so-called block-copolymer (BCP), polymers made up of blocks of different monomeric components.

Intriguingly, BCP tend to self-assemble on nanoscale, in a way which strongly depends by the relative concentration of their different polymeric components. In our case, starting from polystyrene-block-poly-4-vinylpyridine (PS-b-P4VP) BCP we produced micelles loaded with silver nano-particles (Ag-NPs). Through a spin-coating deposition over a glass substrate we obtained a self-assembled isotropic nanostructure with characteristics of homogeneity typical of the so-called near-hyperuniform disorder [Zito et al, 2015]. The resulting highly dense, homogeneous and isotropic random pattern consists of clusters of silver nanoparticles with limited size dispersion.

A typical TEM image of the resulting SERS substrate is shown in Fig. 6. Each nano-island consisted of nearly touching (or in contact) nanoparticles of size in the range ~1–12 nm. The average nano-island diameter was D ~26 nm, the cluster height was h ~ 14 nm, and the hexagonal pattern is characterized by a gap g ~ 2-3 nm between the NP-islands.

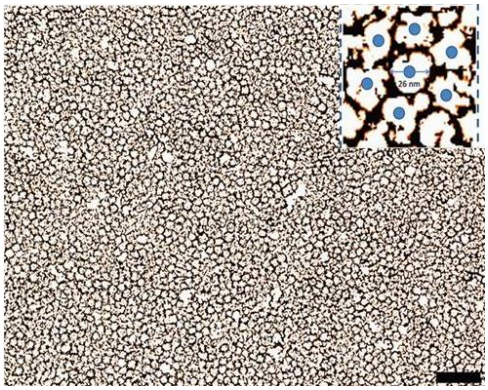

Figure 6: Transmission Electron Microscopy image of self-assembled SERS substrates.
TEM micrograph of the final random pattern obtained by applying our protocol: the filling fraction is highly increased inducing nanoisland gaps of 2–3 nm, as shown in the close-up. Scale bar is 150 nm.

We took advantages of the high spatial reproducibility of our SERS substrates to analyse the RBC membrane. Since the SERS substrate is actually localized only at the cell surface our method is able to discriminate the bio-chemistry composition of the cell membrane. Remarkably, SERS spectra resulted to be characterized by glycoprotein and glycolipid contributions not masked by the resonant membrane-bound Hb (see Fig.7). We are currently expanding the study on red blood cells to discriminate the molecular variation induced at the membrane during the life cycle of the cell and under mechanical stress induced into a microfluidic channel. The same approach will be also used

to study the expression of specific proteins on cancer cells membranes, an information that can be helpful for early diagnosis.

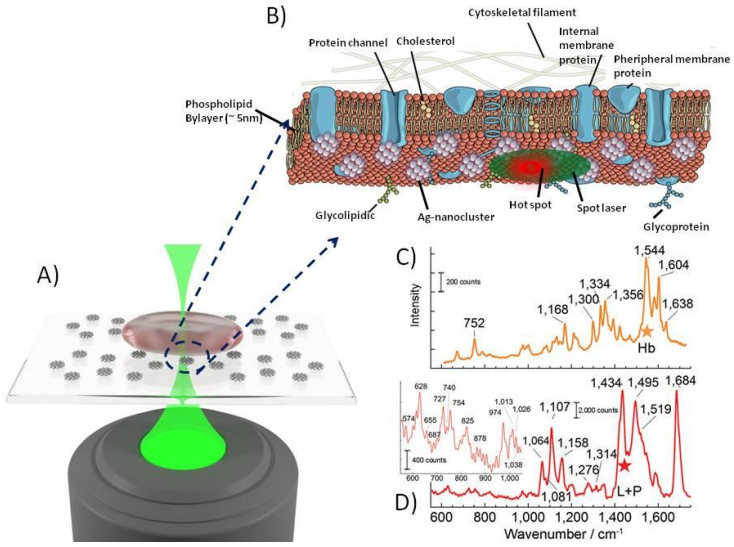

Figure 7: SERS analysis of RBC membrane.
A) the laser beam is focused on a single RBC adhered on a SERS coated or uncoated (not shown in figure) coverslips; B) Zoom on the interface between the SERS substrates and the RBC membrane; C) Spontaneous Raman spectrum of RBC, which shows typical spectral features of hemoglobin; D) Typical SERS spectrum measured at z = 0, which clearly presents spectral markers of membrane lipids and proteins. Inset in D) shows a magnified view of the smaller spectral features.

6. TIP-ENHANCED RAMAN SCATTERING FOR STUDYING BACTERIA SURFACE

Many problems at the frontiers of materials science and biotechnology require a spatial resolution that is outside of the diffraction-limited regime of the conventional optical techniques. Very recently, a new research field has emerged that seems to offer the potential to bridge this gap. This new technique is termed Tip-Enhanced Raman Scattering (TERS). TERS relies on the combination of near-field scanning probe microscopy and enhanced Raman spectroscopy. In TERS, in fact, the near field scanning probe (e.g. the tip of an Atomic Force Microscope, AFM) is covered by metal NPs. In this way, the tip behaves as a sort of optical nano-antenna that gives place to huge amplification

of the optical field as for SERS but only in proximity of the tip apex. Therefore, due the short-range character of plasmon resonance, the enhanced Raman signal can be acquired with a spatial resolution only limited by the tip geometry. Since the radius of curvature of scanning probe tips is of the order of tens of nm, the obtained spatial resolution is well below the light diffraction limit. Hence, TERS acquires simultaneously the topographic structure of the scanned surface but also its bio-chemistry composition, revealed by the tip-enhanced spectrum. A sketch of TERS mechanism is shown in Fig. 8.

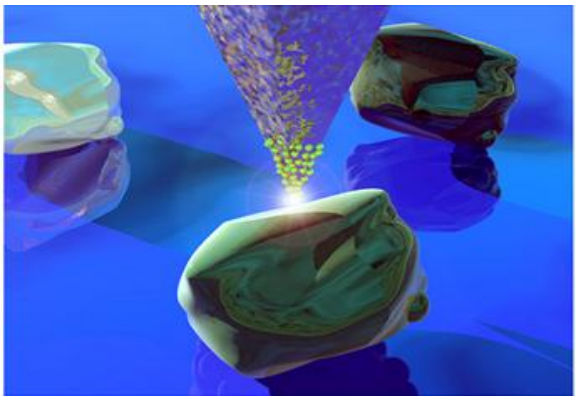

Figure 8: Basic idea of Tip Enhanced Raman Scattering.
A sketch of the basic principle of TERS. A very thin tip of an Atomic Force Microscope is coated with metal nanoparticles and shined by a proper laser wavelength. When the tip approaches the surface of the sample the enhanced optical field allows the detection of also few molecules in the short range of the nano-antenna.

Historically, the first TERS realization dates to 2000 by Kawata and co-workers [Hayazawa et al., 2000], shortly followed by Zenobi's group [Stockle et al., 2000]. These pioneering studies have well elucidated the main TERS features: a very high sensitivity (due to the near-field plasmonic enhancement) combined with an elevated spatial resolution, obtained by the scanning probe-based approach. Both these characteristics make TERS a unique tool, for instance, to directly localize and identify proteins and their conformation in a complex (e.g., native) environment. In addition, it represents an excellent tool for detecting biomolecules that are adsorbed, layered, or assembled on a large variety of surfaces and interfaces, included the outer side of cell membranes.

The simultaneous recording of both topographical and chemical structure achievable by TERS has, over the last years, allowed to reach a deeper insight into the surface properties of many complex systems at the nanoscale, opening

new opportunities for their use as concrete *living biotechnological tools*. Spores, the "dormant" state of bacteria, own to this family.

Recently, we applied TERS spectroscopy for surface analysis of *Bacillus subtilis* spores, a very attractive bio-system for a wide range of applications regulated by the spore surface properties. In particular, these spores have been proposed as mucosal vaccines and proposed as carriers for drug delivery applications.

The observed TERS spectra reflect the complex and heterogeneous environment explored by the plasmonic tip, therefore exhibiting significant point-to-point variations at the nanoscale (see Fig. 9).

Given such molecular complexity, a robust correlative imaging was necessary for eliciting the spore surface chemical information. In particular, by taking advantage of advanced statistical tools such as Principal Components Analysis (PCA), we demonstrated the existence of a denser arrangement of both proteins and carbohydrates on specific spore surface regions (the spore "ridges", see Fig. 9a) simultaneously revealed by AFM imaging [Rusciano et al., 2014]. Intriguingly, the ridge might act as a sort of chemical reservoir for bacteria after sporulation of the dormant cell. Successful TERS analysis of spores' surface constitutes an essential step toward the use of spores for drug delivery applications.

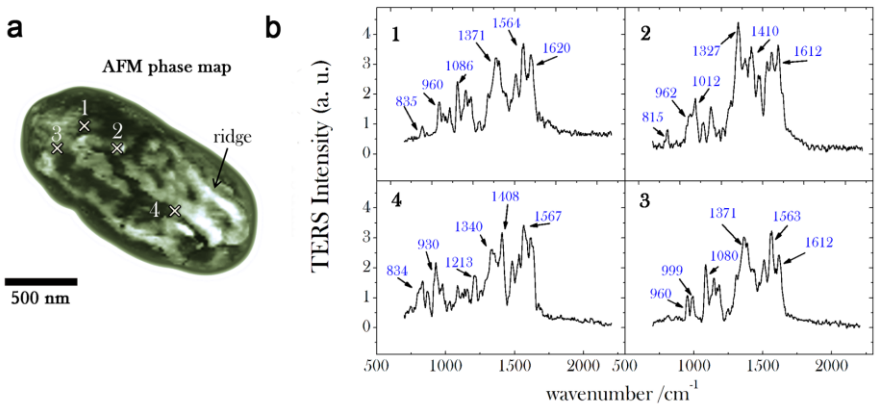

Figure 9: TERS analysis of bacteria spore surface.
(a) AFM phase map of a whole spore acquired in tapping mode (scale bar = 500 nm, step-size = 20 nm).
(b) Near-field (normalized) TERS spectra acquired in four selected positions over the spore coat, corresponding to the cross-marks in (a).

7. REFERENCES

[1] *Biophotonics*, Pavesi L. and Fauchet P. M. (Eds.), Springer-Verlag Berlin Heidelberg (2008).

[2] Rusciano G. (2010) *"Experimental analysis of Hb oxy-deoxy transition in single optically stretched red-blood cells"* Physica Medica: European Journal of Medical Physics **26**, 233-239.

[3] De Luca A.C., Rusciano G., Ciancia R., Martinelli V., Pesce G., Rotoli B. and Sasso A. (2008) "*Spectroscopical and Mechanical Characterization of Normal and Thalassemic Red Blood Cells by Raman Tweezers*" , Opt. Express **16**, 7943.

[4] Rusciano G., De Luca A.C., Pesce G., Oliviero G., Amato J., Borbone N., D'Errico S., Piccialli V., Piccialli G., Mayol L. (2011)*"Label-Free Probing of G-Quadruplex Formation by Surface-Enhanced Raman Scattering"* Anal. Chem. **83**, 6849-6855.

[5] Fleischmann M., Hendra P. J. and McQuillan A. J. (1974) "*Raman spectra of pyridine adsorbed at a silver electrode"* Chem. Phys.Lett., 1974, **26**, 163–166.

[6] Jeanmaire D. L. and Van Duyne R. P. (1977) *"Surface Raman Spectro electrochemistry Part I. Heterocyclic, Aromatic, and Aliphatic Amines Adsorbed on the Anodized Silver Electrode"* J. Electroanal. Chem., **84**, 1–20.

[7] Albrecht M. G. and Creighton J. A. (1977) *"Anomalously intense Raman spectra of pyridine at a silver electrode"* J. Am. Chem. Soc. **99**, 5215–5217.

[8] Zito G., Rusciano G., Pesce G., Dochshanov A., Sasso A. (2015) "*Surface-enhanced Raman imaging of cell membrane by a highly homogeneous and isotropic silver nanostructure*" Nanoscale **7**, 8593-8606.

[9] Hayazawa N., Inouye Y., Sekkat Z., Kawata S. (2000) "*Metallized Tip amplification of near-field Raman scattering*", Opt. Commun.; **183**, 333–6.

[10] Stockle R.M., Suh Y.D., Deckert V., Zenobi R. (2000) "*Nanoscale chemical analysis by tip-enhanced Raman spectroscopy*", Chem. Phys. Lett. **318**, 131–6.

[11] Rusciano G., Zito G., Isticato R., Sirec T., Ricca E., Bailo E., Sasso A. (2014) "*Nanoscale chemical imaging of bacillus subtilis spores by combining Tip-Enhanced Raman Scattering and advanced statistical tools*" ACS Nano **8,** 12300-12309.